


Article

# Influence of Preparation Conditions on the Catalytic Performance of Mo/H-ZSM-5 for Methane Dehydroaromatization

Maria Teresa Portilla<sup>1,2</sup>, Francisco J. Llopis<sup>3</sup>, Manuel Moliner<sup>1</sup> and Cristina Martínez<sup>1,\*</sup> 

<sup>1</sup> Instituto de Tecnología Química (UPV-CSIC), Universitat Politècnica de València—Consejo Superior de Investigaciones Científicas, Av. De los Naranjos s/n, 46022 Valencia, Spain; Teresa.Portilla@iff.com (M.T.P.); mmoliner@itq.upv.es (M.M.)

<sup>2</sup> Technical Department of International Flavors & Fragrances (IFF), Av. Felipe Klein 2, 12580 Benicarló, Spain

<sup>3</sup> Departamento Ingeniería Química, Universitat de València (UV), Av Universidad s/n, 46100 Burjassot, Spain; francisco.llopis@uv.es

\* Correspondence: cmsanche@itq.upv.es

**Abstract:** Methane, the main component of natural gas, is an interesting source of chemicals and clean liquid fuels, and a promising alternative raw material to oil. Among the possible direct routes for methane conversion, its aromatization under non-oxidative conditions has received increasing attention, despite the low conversions obtained due to thermodynamic limitations, because of its high selectivity to benzene. Mo/H-ZSM-5, the first bifunctional zeolite-catalyst proposed for this reaction, is still considered as one of the most adequate and has been widely studied. Although the mono- or bifunctional nature of the MDA mechanism is still under debate, it is generally accepted that the Mo species activate the C-H bond in methane, producing the intermediates. These will aromatize on the Brønsted acid sites of the zeolite, whose pore dimensions will provide the shape selectivity needed for converting methane into benzene. An additional role of the zeolite's Brønsted acid sites is to promote the dispersion of the Mo oxide precursor. Here, we show the influence of the different preparation steps—metal incorporation, calcination and activation of the Mo/ZSM-5- on the metal dispersion and, therefore, on the activity and selectivity of the final catalyst. Metal dispersion is enhanced when the samples are calcined under dynamic conditions (DC) and activated in N<sub>2</sub>, and the benefits are larger when the metal has been incorporated by solid state reaction (SSR), as observed by FESEM-BSE and H<sub>2</sub>-TPR. This leads to catalysts with higher activity, increased aromatic selectivity and improved stability towards deactivation.

**Keywords:** methane aromatization; zeolites; Mo/ZSM-5; catalysts preparation; catalyst activation



**Citation:** Portilla, M.T.; Llopis, F.J.; Moliner, M.; Martínez, C. Influence of Preparation Conditions on the Catalytic Performance of Mo/H-ZSM-5 for Methane Dehydroaromatization. *Appl. Sci.* **2021**, *11*, 5465. <https://doi.org/10.3390/app11125465>

Academic Editor: Chang Geun Yoo

Received: 30 April 2021

Accepted: 8 June 2021

Published: 12 June 2021

**Publisher's Note:** MDPI stays neutral with regard to jurisdictional claims in published maps and institutional affiliations.



**Copyright:** © 2021 by the authors. Licensee MDPI, Basel, Switzerland. This article is an open access article distributed under the terms and conditions of the Creative Commons Attribution (CC BY) license (<https://creativecommons.org/licenses/by/4.0/>).

## 1. Introduction

The chemical industry is rapidly evolving towards the use of more efficient and sustainable processes. Two key factors in this line are the application of heterogeneous catalysts, on the one hand, and the use of alternative raw materials, on the other. Regarding the substitution of conventional feedstocks, such as oil or coal by others, environmentally friendlier, this can be approached in two different ways. One of them is the recycling and upgrading of waste materials as one of the possible routes for contributing to a circular economy by reducing the exploitation of natural resources. Some of these wastes are plastics [1–3] and biomass derivatives [4–6], which can be used for the production of chemical building blocks, such as olefins and aromatics, or fly ash that can be transformed into nanoporous materials with different applications. The other option is the substitution of oil and coal by methane, major component of natural gas, which, despite its fossil origin, presents a higher hydrogen to carbon (H/C) ratio and a smaller environmental footprint than oil [7–10]. The interest in methane as an alternative raw material has increased

substantially due to the recent discovery of large reserves of shale gas, coalbed methane and methane clathrates, resulting in a high availability and low cost of natural gas [11–16].

There are two main routes for methane conversion, e.g., by means of indirect or direct processes. The indirect conversion of methane to chemicals and fuels through the intermediate formation of the more reactive synthesis gas mixture (syngas, CO + H<sub>2</sub>), a mixture of H<sub>2</sub> and CO obtained by reforming or partial oxidation, is currently the only process industrially applied [17–19]. Syngas is then converted, in a second step, to hydrocarbons by means of the Fischer–Tropsch synthesis [15,20–22], into light olefins or gasoline with methanol as an intermediate [15], or into DME in a single stage [20]. However, these indirect routes involve high energy requirements and, consequently, large CO<sub>2</sub> emissions, and this has led to an active research into alternative processes for the direct conversion of methane into hydrocarbons of interest [8], despite the challenge associated to the high chemical stability of the methane molecule. Direct methane upgrading can be approached under oxidative and non-oxidative conditions [15,20,22]. The oxidative routes involve the use of oxygen, which is beneficial, as it will increase the reaction rate by shifting the thermodynamic equilibrium. However, kinetically it will limit the yields to the desired primary products that are much more reactive than methane under the experimental conditions used, and which will be further converted into combustion products. This has prevented the commercial application of the oxidative methane conversion processes so far [21]. Given the limitations of the oxidative processes, the methane dehydroaromatization reaction (MDA) has gained interest in the last decades [23,24] because of its high selectivity to hydrocarbons, mainly ethylene and benzene, which are of great interest as a raw material for the petrochemical industry, and the additional production of hydrogen.

Methane dehydroaromatization takes place in the presence of bifunctional catalysts based on transition metal loaded acid zeolites. Among the different metals proposed, Mo is the best performing and has been the most studied [25]. Regarding the zeolites, medium pore structures with pore dimensions close to the dynamic diameter of benzene, the desired product [23], are the most selective [26,27]. Among the 10-ring zeolites, ZSM-5 [28–31] and MCM-22 [30,32–38] have been thoroughly studied and are the most efficient in terms of benzene yield and catalyst life. However, other medium pore zeolites have also been reported as active for MDA, such as IM-5 [39–41] or TNU-9 [41,42].

Regarding the reaction mechanism and the active sites involved, it is widely accepted that methane is first activated on the Mo sites and that the reaction intermediates formed will further oligomerize, cyclate and dehydrogenate on the Brønsted acid sites [34,43–49]. In the last few decades, a large effort has been made trying to identify the active species, as well as their formation and how these are affected by the physical-chemical properties of the zeolite used as support [50–56]. Moreover, according to the literature, the incorporation procedure of the molybdenum into the zeolitic material can have an important impact on the physico-chemical properties of the final Mo/zeolite catalyst [49,57]. Although different procedures have been described to prepare the Mo/ZSM-5 catalysts, the most employed technique for Mo incorporation is the incipient wetness using ammonium heptamolybdate (AHM) as the metal precursor [43]. The large [Mo<sub>7</sub>O<sub>24</sub><sup>6-</sup>] anions are located mainly on the external surface of the zeolite [58], and the MoO<sub>3</sub> crystals are formed by calcination at temperatures in the range of 623 to 773 K. Iglesia et al. [50,55,59] proposed the preparation of the Mo/ZSM-5 catalyst by solid state ion-exchange, by physically mixing molybdenum trioxide with the zeolite followed by a calcination step that will force the migration of the Mo species from the external surface into the zeolite micropores. The cationic Mo species, anchored to the zeolite framework, have been identified as the active sites responsible for the selective conversion of methane into aromatics, whereas the presence of Mo clusters at the external surface of the zeolite has been related to the formation of coke [49].

Although a proper dispersion degree and location of the Mo-oxo species has been shown to be key for an optimum methane conversion and benzene selectivity, the active sites are not the starting oxides, but the Mo-oxo-carbide species formed by reduction of the former by the methane feed in the first stage of the MDA process [47,60,61]. Thus,

the reducibility of the starting Mo-oxo species, directly related to their size and location, will play a determinant role. Regarding the contribution of the Brønsted acid sites (BAS), they are known to promote the dispersion of the metal species into the zeolite micropores [62]. Although not essential for dehydroaromatization, as evidenced by Hensen [63], the BAS also enhance the conversion of the intermediates formed on the Mo-species into the desired aromatics [59,64,65]. Recent studies propose the contribution of a hydrocarbon pool mechanism to the MDA reaction [46–48,66,67], similar to the one described for the methanol-to-hydrocarbon (MTH) process.

In the present work, we have studied the influence of the different preparation steps on the physico-chemical properties of the final Mo/ZSM-5 catalyst and, consequently, on their catalytic performance for the MDA reaction. The same parent ZSM-5 zeolite and Mo content (6 wt. %) have been used in all cases, so that the location and dispersion of the metal will only depend on the preparation procedure. Thus, on the one hand two Mo incorporation methodologies have been compared, incipient wetness (IW) and solid-state reaction (SSR). On the other, these two samples have been calcined in a muffle, under a static air atmosphere (SC—static calcination) or in a fixed bed reactor under air flow (DC—dynamic calcination). An additional N<sub>2</sub> treatment will be shown to be beneficial when the samples are prepared by SSR, as it favors the reduction of the MoO<sub>3</sub> clusters, their dispersion on the external surface, and the migration of Mo-species into the micropores of the zeolite and leading to the best performing catalysts among the four compared, in good agreement with previous results reported by Bao [68] and Sedel'nikova [69].

## 2. Experimental Section

### 2.1. Catalyst Preparation

Four Mo/ZSM-5 (6 wt. % Mo) were prepared using a commercial ZSM-5 sample with Si/Al molar ratio of 10 (TZP302A, supplied by TRICAT Catalysts Technologies, acquired by Süd-Chemie, now Clariant, <https://www.clariant.com>, accessed on 11 June 2021) as acid support. This zeolite, originally in its ammonium form, has a heterogeneous crystal size distribution (see Figure S1), an average crystal size close to 1 μm, and is denoted as Z5. The Mo-loaded catalysts have been prepared following two different metal incorporation procedures, e.g., incipient wetness impregnation (IW) and solid-state ion exchange reaction (SSR). The metal precursor employed for the incipient wetness impregnation is ammonium heptamolybdate tetrahydrate (99% Merck, (NH<sub>4</sub>)<sub>6</sub>Mo<sub>7</sub>O<sub>24</sub>·4 H<sub>2</sub>O). After impregnation, the catalyst was dried at 373K overnight followed by a calcination in air at 773 K for 3 h, under static conditions in a muffle (MoZ5-IW-SC) or under dynamic conditions in a fixed-bed reactor (MoZ5-IW-DC). For the solid state reaction, the zeolite was physically mixed with molybdenum (VI) oxide (≥99.5% MoO<sub>3</sub>, Sigma-Aldrich, <https://www.sigmaaldrich.com>, accessed on 11 June 2021) and calcined in air at 723 K for 10 h in a muffle (Mo-Z5-SSR-SC) or in a fixed-bed reactor (MoZ5-SSR-DC). Part of the two catalysts prepared by SSR has been pre-treated in nitrogen (15 mL/min), by heating from room temperature (Tr) to 923 K at a rate of 10 K/min and cooling down to Tr. These nitrogen-treated samples have been labelled as MoZ5-SSR-SC-N<sub>2</sub> and MoZ5-SSR-DC-N<sub>2</sub>.

### 2.2. Characterization Methods

Fresh catalysts were characterized by X-ray power diffraction (XRD) recorded in a Philips X'Pert diffractometer equipped with a graphite monochromator, operating at 40 kV and 45 mA, and using nickel-filtered Cu Kα radiation (λ = 0.1542 nm).

The bulk chemical composition of the catalysts was analyzed in a 715-ES ICP-Optical Emission spectrometer, after dissolution of the solids in a HNO<sub>3</sub>/HF solution.

Textural properties were determined from the nitrogen adsorption isotherm, measured at 77 K on a Micrometrics ASAP 2010 volumetric adsorption analyzer. Surface area and micropore volume values were obtained by applying the BET equation [70] and from the t-plot graph [71], respectively.

The relative concentration of acidic sites in the different samples was obtained by FT-IR spectroscopy using pyridine as the probe molecule. Pyridine adsorption–desorption experiments were carried out on self-supported wafers (10 mg/cm) of samples activated at 673 K and  $10^{-2}$  Pa for 2 h. After wafer activation, the base spectrum was recorded, and pyridine vapor ( $6.5 \times 10^2$  Pa) was admitted into the vacuum IR cell and adsorbed onto the zeolite. Desorption was performed in vacuum over three consecutive 1-h periods of heating at 523, 623, and 673 K, each followed by an IR measurement at room temperature. All the spectra were scaled according to the sample weight. The amount of Brønsted and Lewis acid sites (BAS and LAS, respectively) was determined from the intensities of the bands at ca. 1545 and 1450  $\text{cm}^{-1}$ , respectively, using the molar extinction coefficients given by Emeis [72].

Metal dispersion of the Mo/ZSM-5 catalysts was examined by field emission scanning electron microscopy (FESEM) equipped with backscatter electron (BSE) detector on a ZEISS ULTRA 55 microscope operating at 2 kW.

Temperature-programmed reduction ( $\text{H}_2$ -TPR) was performed in a Micromeritics Autochem 2910. The sample (100 mg) was pre-treated in argon flow at room temperature for 30 min, then the gas was switched to the reduction mixture (10 wt. %  $\text{H}_2$  in Ar) with a flow rate of 50 mL/min, and temperature was increased to 1373 K at a heating rate of 10 K/min. The  $\text{H}_2$  consumption was followed by a thermal conductivity detector (TCD). No sublimation of molybdenum species was observed during the  $\text{H}_2$ -TPR experiments, in agreement with previous descriptions [73].

### 2.3. Catalytic Testing

Dehydroaromatization of methane was performed in a continuous down-flow fixed-bed reactor, at atmospheric pressure, 973 K and a contact time (w/F) of 16 g cat·h/mol  $\text{CH}_4$ , adjusted to a catalyst weight of 0.5 g diluted with silicon carbide to a constant bed volume of 2.8  $\text{cm}^3$ . The catalyst was activated by heating from room temperature to 923 K in methane atmosphere ( $\text{CH}_4:\text{N}_2 = 80:20$  in vol. %), and purging in nitrogen flow for 30 min at this temperature. Then the feed was switched again to methane ( $\text{CH}_4:\text{N}_2 = 80:20$  in vol. %) for starting the reaction that was continued out for 18 h.

The reactor outlet stream was analyzed online by means of a gas chromatograph (Bruker GC-450) provided with two independent channels and three detectors. The permanent gases ( $\text{N}_2$  as internal standard,  $\text{H}_2$ , CO,  $\text{CO}_2$ ) and  $\text{CH}_4$  are analyzed in a first channel equipped with a TCD and three columns, a Hayesep N (0.5 m length), a Hayesep Q (1.5 m) and a 13X molecular sieve (1.2 m length). In a second channel the C1-C4 hydrocarbons were first separated from the aromatics in a CP-Wax capillary column (5.0 m length and 0.32 mm inner diameter). Then, the light gases were directed to a CP-Porabond Q (25 m length and 0.32 mm inner diameter) connected to a FID, and the aromatics were directed to a second CP-Wax (1.0 m length and 0.32 mm inner diameter) connected to a second FID.

Yields and selectivities to the different products were given on a carbon basis. The amount of carbonaceous deposits on the catalyst was calculated as the difference between the carbon at the inlet and at the outlet of the reactor as determined from the on-line GC analyses, by co-feeding  $\text{N}_2$  (20 mol. %) as internal standard.

## 3. Results and Discussions

### 3.1. Characterization Results

Incorporation of 6 wt. % of molybdenum was confirmed by ICP for all of catalysts resulting in a Mo/Al molar ratio of 0.5 (see Table 1), independently of the metal incorporation method (incipient wetness impregnation, IW, or solid state reaction, SSR) or the calcination procedure (muffle or fixed-bed reactor). This Mo/Al molar ratio was reported by Borry et al. [50] to be the optimum for activating the methane molecules on the active Mo species and converting them to aromatics on the BAS.

The preservation of the zeolitic structure after Mo incorporation was confirmed by powder XRD (see Figure 1). It is important to note that the PXRD patterns of the samples

prepared by solid state reaction, MoZ5-SSR-SC and MoZ5-SSR-DC, present some peaks assigned to MoO<sub>3</sub> at 12.3°, 25.7°, 27.4° and 39°, indicating the presence of larger oxide agglomerates. These peaks are more intense when the samples were obtained by muffle calcination (MoZ5-SSR-SC). However, no diffraction peaks corresponding to MoO<sub>3</sub> were detected in the samples prepared by incipient wetness (IW), independently of the calcination procedure, indicating a better dispersion of the metallic species.

**Table 1.** Physico-chemical properties of the Mo/ZSM-5 catalysts.

Sample	ICP			S <sub>BET</sub> (m <sup>2</sup> /g)	S <sub>micro</sub> (m <sup>2</sup> /g)	V <sub>micro</sub> (cm <sup>3</sup> /g)
	Si/Al	Mo/Al	Mo (wt. %)			
Z5 (TZP302A)	10.0	—	—	368	355	0.17
MoZ5-IW-SC	10.5	0.5	6.0	270	257	0.12
MoZ5-IW-DC	9.9	0.5	6.1	263	246	0.12
MoZ5-SSR-SC	10.3	0.5	6.4	292	275	0.13
MoZ5-SSR-DC	10.2	0.5	6.3	276	260	0.13
MoZ5-SSR-SC-N2	10.3	0.5	6.4	254	241	0.12
MoZ5-SSR-DC-N2	10.2	0.5	6.3	237	221	0.11

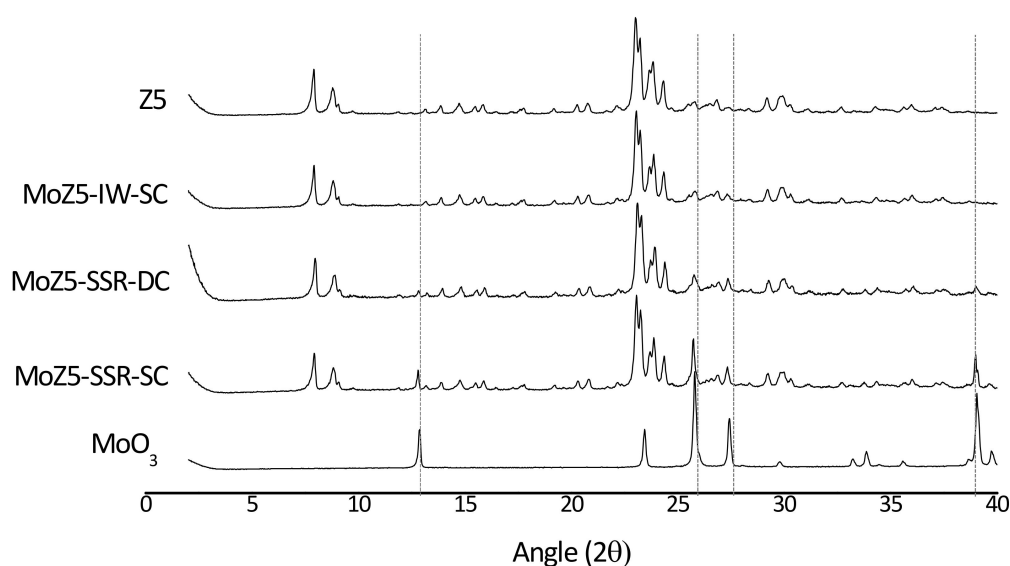


**Figure 1.** PXRD patterns of the Mo/ZSM-5 catalysts. The most characteristic peaks related to the presence of MoO<sub>3</sub> are marked with a dotted line.

The presence of large MoO<sub>3</sub> particles in the two samples prepared by SSR, MoZ5-SSR-SC and MoZ5-SSR-DC, is confirmed by FESEM employing a backscatter electron (BSE) detector (see Figure 2).

The Mo-loaded ZSM-5 samples present lower BET surface area, micropore surface area and volume, (see Table 1 and isotherms in Figure S2 in the Supplementary Materials) and a lower amount of total Brønsted acid sites (see Table 2) as compared to the parent zeolite. This fact could be related to the partial blocking of the zeolite microporosity by the MoO<sub>3</sub> particles and to the migration of the Mo species into the channels during the calcination step, as previously described [46,54,60], a migration that has been directly related to the presence of Brønsted acid sites [50,54,58,59,62,63,74]. As expected, the metal incorporation procedure has an important influence on the textural and acidic properties of the final catalysts, and the higher the metal dispersion according to PXRD and FESEM, the larger the reduction of micropore surface and BAS density, in good agreement with previous publications [49,69].

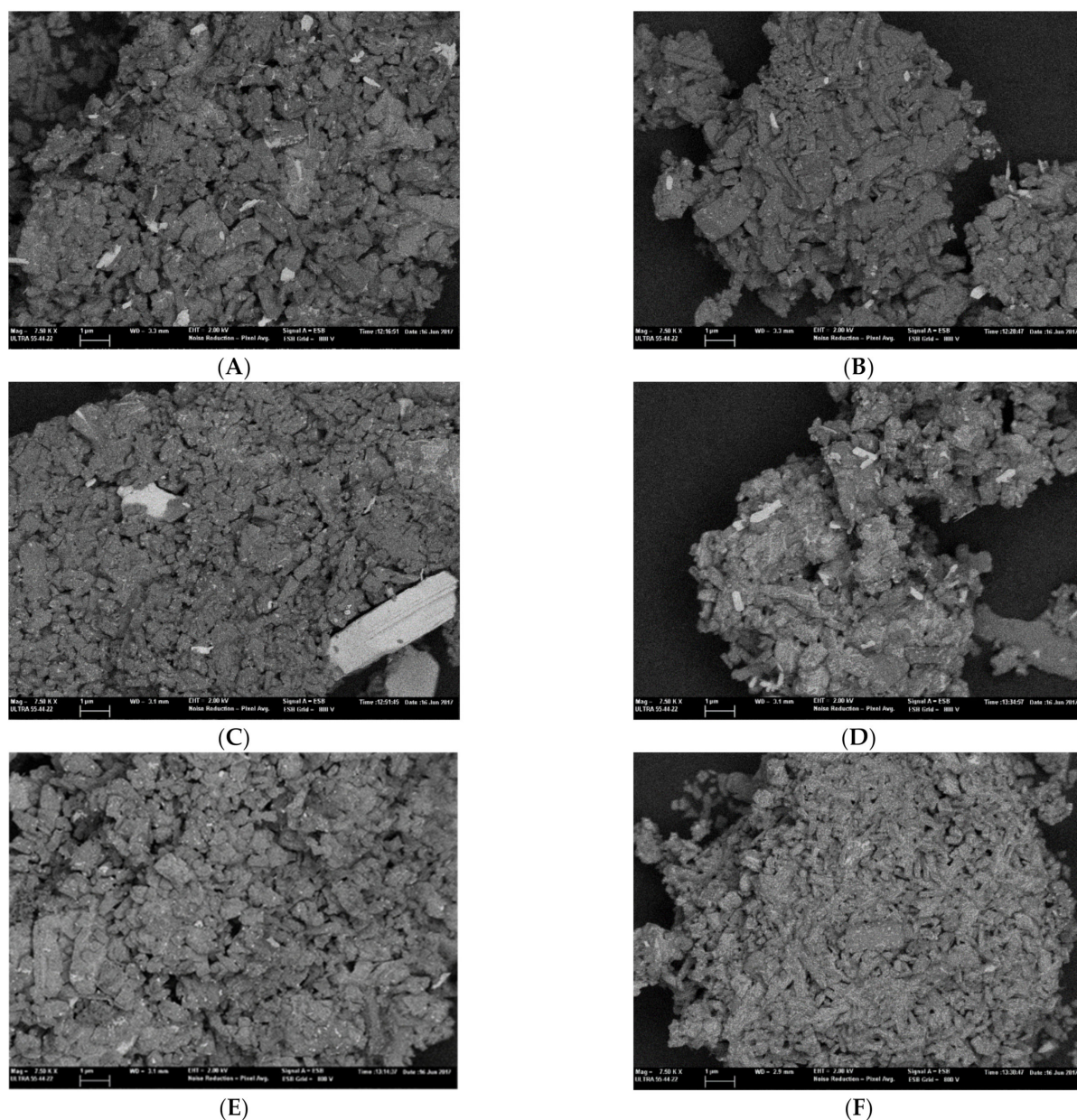


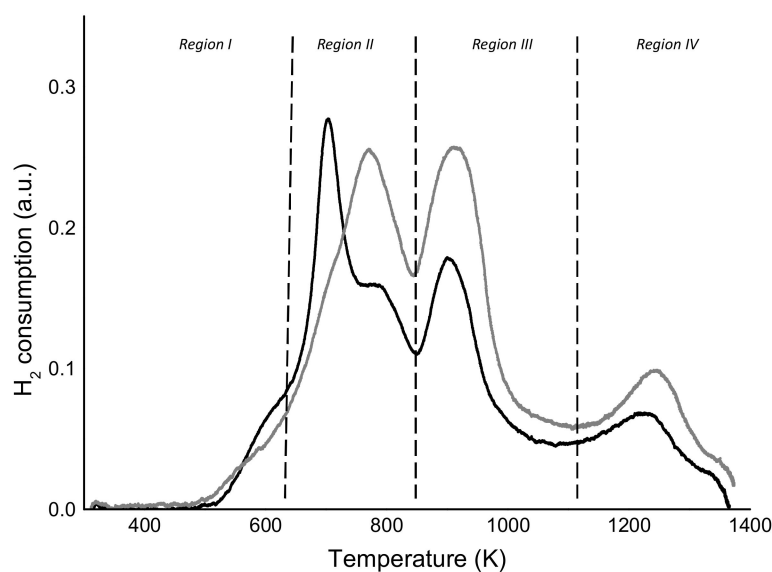
**Figure 2.** FESEM images of the Mo/ZSM-5 catalysts by a field emission scanning electron microscopy employing a backscatter electron detector (BSE): (A) MoZ5-IW-SC, (B) MoZ5-IW-DC, (C) MoZ5-SSR-SC, (D) MoZ5-SSR-DC, (E) MoZ5-SSR-SC-N2, (F) MoZ5-SSR-DC-N2.

**Table 2.** Acidic properties of the Mo/ZSM-5 catalysts.

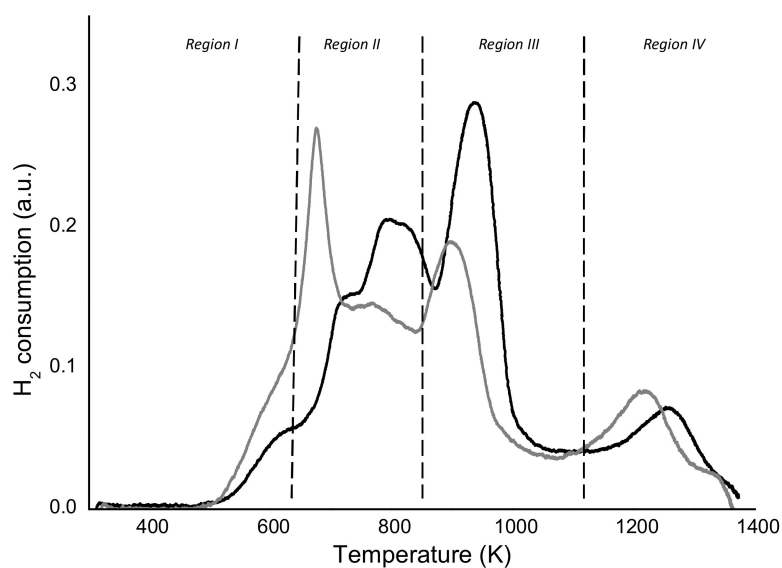
Sample	Brønsted Acidity (mol Py/g)				Lewis Acidity (mol Py/g)		
	B523	B623	B673	B673/B523	L523	L623	L673
Z5 (TZP302A)	564	368	241	0.43	7	0	0
MoZ5-IW-SC	213	122	107	0.50	23	14	3
MoZ5-IW-DC	199	150	65	0.32	21	13	0
MoZ5-SSR-SC	295	184	116	0.39	31	19	9
MoZ5-SSR-DC	250	138	124	0.50	13	5	5
MoZ5-SSR-SC-N2	237	132	95	0.40	37	25	18
MoZ5-SSR-DC-N2	236	131	100	0.42	32	21	19

Since the dispersion of molybdenum depends on the Mo incorporation method, it may also interfere in the nature, the accessibility and the reducibility of the Mo species. Indeed, not only the impregnation method but also the calcination mode altered the H<sub>2</sub>-TPR profile of the Mo/ZSM-5 samples (see Figure 3). According to the literature [52,75,76], four regions can be distinguished based on the Mo reduction temperature, a low temperature region in the range of 473–650 K (I) related to the partial reduction of amorphous polymeric molybdate species, a second region (II, 650–875 K) ascribed to the reduction of MoO<sub>3</sub> to MoO<sub>2</sub>, a third one (III, 875–1173 K) assigned to the reduction of MoO<sub>2</sub> to MoO, and a high temperature region (IV, T > 1173 K) related to the reducibility of the [Mo<sub>2</sub>O<sub>3</sub>]<sup>+2</sup> species occluded inside the zeolitic channels, which are more difficult to be reduced. The main differences among the four catalysts are related to the reduction profiles in regions II and III. Thus, MoZ5-IW-SC presents two peaks in region II at 700 and 760 K, assigned to the reduction of MoO<sub>3</sub> particles on the external surface, easily reducible, and within the zeolite pores, to MoO<sub>2</sub>. A lower H<sub>2</sub> consumption in region III suggests that not all the Mo<sup>4+</sup> species formed and observed in region II are susceptible to further reduction. Sample MoZ5-SSR-DC presents a very similar profile, although the peak maximums are slightly shifted to lower temperatures. However, sample MoZ5-SSR-SC, prepared by solid-state reaction but calcined in a muffle, presents the region II and region III peaks shifted to higher temperatures and in different proportions as those observed for MoZ5-IW-DC. These higher reduction temperatures of sample MoZ5-SSR-SC could be related to the presence of large MoO<sub>3</sub> species, as observed by FESEM (see Figure 2), more difficult to be reduced than small MoO<sub>3</sub> particles, highly dispersed on the zeolite surface. However, once this first reduction occurs, a larger peak is observed in Region III indicating a higher H<sub>2</sub> consumption, which could be attributed to a dispersion of the large Mo agglomerates under the H<sub>2</sub>-TPR conditions (H<sub>2</sub> flow and increasing temperature) facilitating the reduction of these new Mo species formed. The reduction in size of the Mo particles on the MoZ5-SSR-SC sample after H<sub>2</sub>-TPR measurement was confirmed by SEM (see Figure S3 in the Supplementary Materials), indicating that, indeed, exposure of the sample to the measurement conditions led to a dispersion of the Mo species.

The fourth sample, MoZ5-IW-DC, prepared by incipient wetness and calcined in air flow, presents two peaks with similar intensities in regions II and III, suggesting that all the MoO<sub>3</sub> species that are first reduced to MoO<sub>2</sub> are further reduced in a second step. Moreover, the region II peak is more symmetric and shifted towards higher temperature as compared to the profile obtained for the IW sample calcined in a muffle, suggesting a more homogenous speciation of the Mo sites and an enhanced migration of the Mo species into the zeolite micropores. All catalysts present analogous reduction bands in regions I and IV, but the intensity of the region IV peaks varies depending on the calcination procedure, and the samples calcined in air flow (DC) present higher hydrogen consumption at high temperature indicating that a larger proportion of Mo species have migrated inside of the zeolitic channels during the calcination step.



(a)



(b)

**Figure 3.** H<sub>2</sub>-TPR profiles for the Mo/ZSM-5 catalyst prepared by incipient wetness, MoZ5-IW-SC (black line), and MoZ5-IW-DC (grey line) (a) and by solid state reaction, MoZ5-SSR-SC (black line) and MoZ5-SSR-DC (grey line) (b).

If exposure to a H<sub>2</sub> flow during the H<sub>2</sub>-TPR measurement resulted in an increased dispersion of the Mo species for catalyst MoZ5-SSR-SC, a similar improvement could be expected for the other catalyst prepared by solid ion exchange, MoZ5-SSR-DC. Thus, the two SSR samples were treated by controlled temperature increase from Tr to 973 K under N<sub>2</sub> flow and cooled down for characterization and testing. The N<sub>2</sub>-treatment results in a reduction of the BET and micropore surface area in both cases (see Table 1), suggesting a further dispersion and migration of the Mo species into the zeolite structure, which is confirmed by FESEM combined with a BSE detector, as shown in Figure 2E,F. With



this additional step, the two SSR catalysts become also more similar to those prepared by IW in terms of their textural properties and, in good agreement with the electron microscopy results, the diffraction peaks corresponding to  $\text{MoO}_3$ , present in the XRD pattern of the two MoZ5-SSR catalysts, disappear after the  $\text{N}_2$  treatment (See Figure S4 in the Supplementary Materials).

The BAS density of the samples is also reduced with the additional  $\text{N}_2$  treatment, and the decrease is larger for the sites able to retain pyridine at the two highest temperatures, 623 and 673 K (see Table 2). An increase of the LAS density is also observed, confirming the formation of cationic Mo species replacing the proton at the original BAS and creating new LAS, as reported by Vollmer et al. [49].

The  $\text{N}_2$  treatment also affects the reducibility of the Mo species of the samples prepared by SSR, and the profiles of the treated SSR samples are now comparable in shape and in  $\text{H}_2$  consumption to the one presented by the catalyst prepared by incipient wetness (see Figure S5 in the Supplementary Materials).

### 3.2. Catalytic Results

In the former section, we have evidenced the impact of the Mo incorporation method on the physico-chemical properties of the final Mo/ZSM-5 catalyst and how the use of an additional pretreatment under  $\text{N}_2$  flow can reduce the size of the larger  $\text{MoO}_3$  particles and favor the formation and/or migration of cationic Mo species into the zeolite micropores. As a direct consequence of their different textural and acidic properties and of the reactivity of their Mo species, the catalysts are expected to differ also in their catalytic performance.

Before starting with the catalytic discussion, however, we would like to note that the catalysts have been activated increasing temperature in methane atmosphere ( $\text{CH}_4:\text{N}_2 = 80:20$  in vol.%). In this way, the  $\text{MoC}_x\text{O}_y$  active species, responsible for the activation of the methane molecules [43,77] are formed before the reaction temperature (973K) is reached. As described in Section 2.3, this stage is followed by 30 min in  $\text{N}_2$  flow before starting to feed the methane mixture. The purpose of this pre-treatment is to have a fully active catalyst, with molybdenum oxo-carbides species already formed, when starting the MDA reaction, and to avoid the competition of both processes [41].

Methane conversion and the hydrocarbon yields versus time on stream (TOS) for the four catalysts obtained by IW and SSR and calcined in air under static (SC) or dynamic conditions (DC) are shown in Figure 4. The initial methane conversion obtained in all cases is around 13%, close to the equilibrium conversion determined by means of Aspen Hysys<sup>®</sup> v.8.0 for a temperature of 973 K using the Gibbs free energy minimization approach, and in good agreement with the values given in the literature [24,41,78].

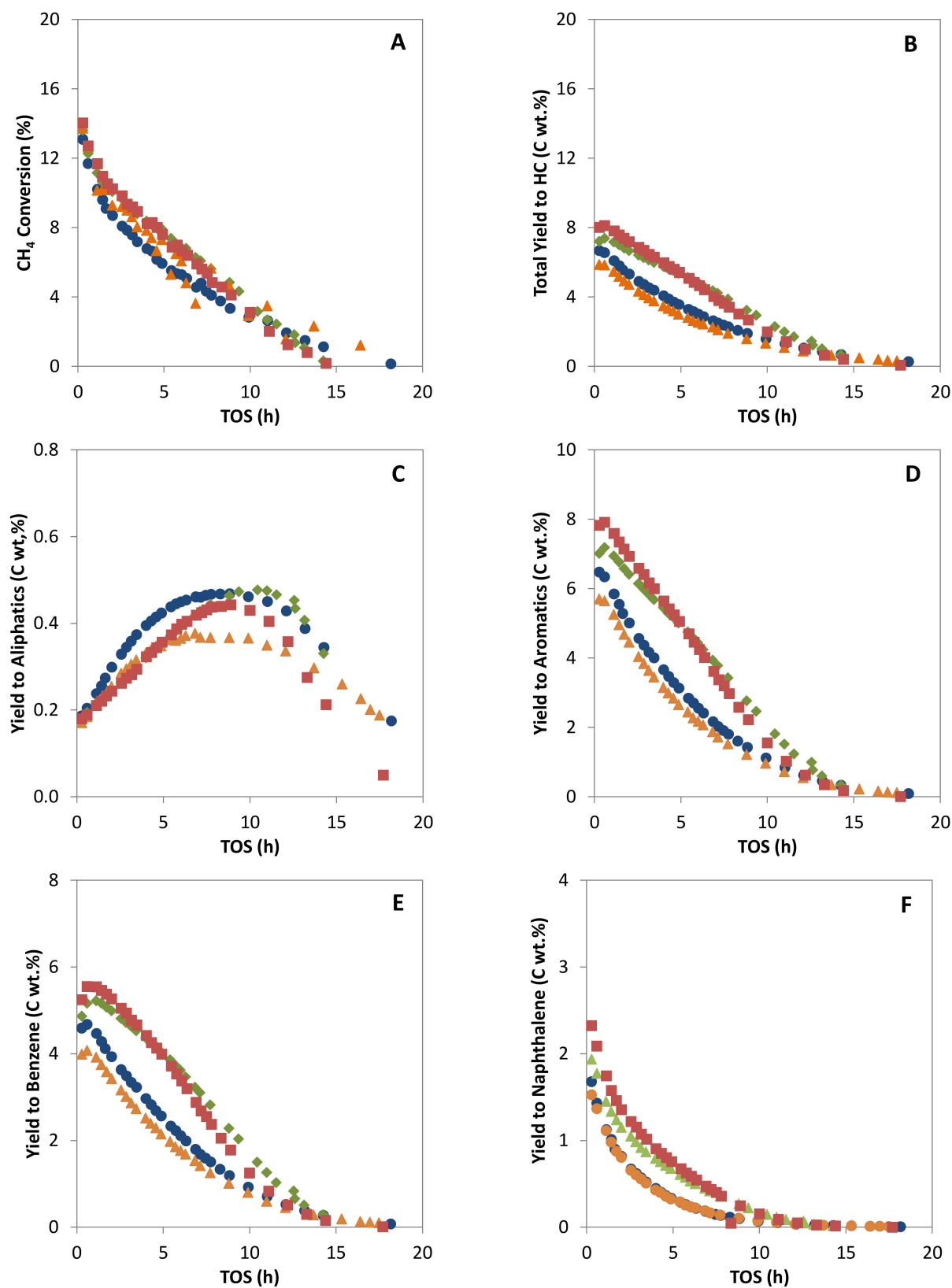


**Figure 4.** Methane conversion (A), total yield to hydrocarbons products (B), yield to aliphatic hydrocarbons (C), to aromatic hydrocarbons (D), to benzene (E) and to naphthalene (F) versus TOS for catalysts MoZ5-SSR-SC (▲), MoZ5-SSR-DC (■), MoZ5-IW-SC (Definitions/applsci-1225460-i002.pdf), and MoZ5-IW-DC (●), at 973 K, atmospheric pressure and  $w/F = 16 \text{ g}\cdot\text{h}/\text{mol}$ .

Despite the comparable initial conversion, the two catalysts obtained by calcination under static conditions, MoZ5-IW-SC and MoZ5-SSR-SC, present a higher deactivation rate and a significantly lower yield to hydrocarbons (see Figure 4A,B, respectively) as compared to the catalysts calcined in N<sub>2</sub> flow (DC). This lower yield to hydrocarbons results from an important reduction of the aromatics and, in particular, of the benzene production (see Figure 4D,E). Moreover, the catalyst obtained by solid ion exchange and calcined in the muffle (MoZ5-SSR-SC) presents the highest coke yields (see Figure 5), as could be expected from the presence of large MoO<sub>3</sub> crystals on the external surface of the zeolites, which, according to the literature [49], are responsible for the formation of coke. On the other hand, the two catalysts obtained by calcination under N<sub>2</sub> flow after Mo incorporation, MoZ5-IW-DC and MoZ5-SSR-DC, present higher yields to aromatics, slightly higher for the latter at short times on stream. This better performance could be related to the improved dispersion of the Mo species and the larger proportion of Mo within the channels, as evidenced by the H<sub>2</sub> consumption in region IV observed by H<sub>2</sub>-TPR.

According to the results presented in the former section, the Mo/ZSM-5 samples prepared by solid state reactions were improved in terms of Mo dispersion after N<sub>2</sub> pretreatment, with their properties becoming more similar to those presented by the samples prepared by IW impregnation. The activity of the N<sub>2</sub>-pretreated SSR catalysts is similar to those of the non-pretreated samples (see Figure 6), but the total yield to hydrocarbons is significantly increased in both cases due to an important increase in the production of benzene. Moreover, coke yield is reduced to values lower than those obtained with the catalysts prepared by IW yield (see Figure 7). Thus, a catalyst with optimum Mo dispersion and BAS density has been obtained by combination of the solid-state reaction method for Mo incorporation and calcination under air flow conditions with a pretreatment in N<sub>2</sub> flow presents the highest activity for methane conversion and benzene production.

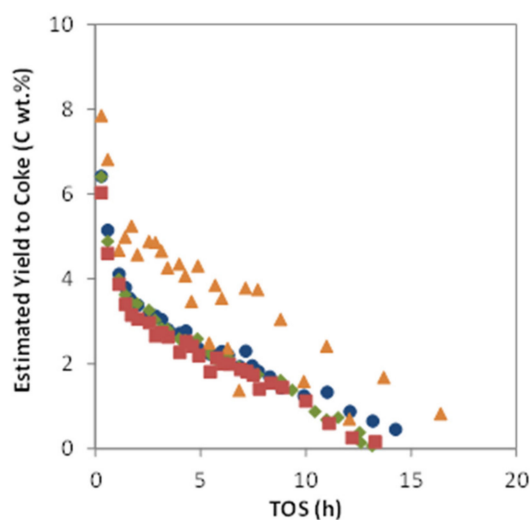


**Figure 5.** Estimated yield to coke versus TOS for catalysts MoZ5-SSR-SC (▲), MoZ5-SSR-DC (■), MoZ5-IW-SC (Definitions/applsci-1225460-i006.pdf), and MoZ5-IW-DC (◆), at 973K, atmospheric pressure and w/F = 16 g·h/mol.

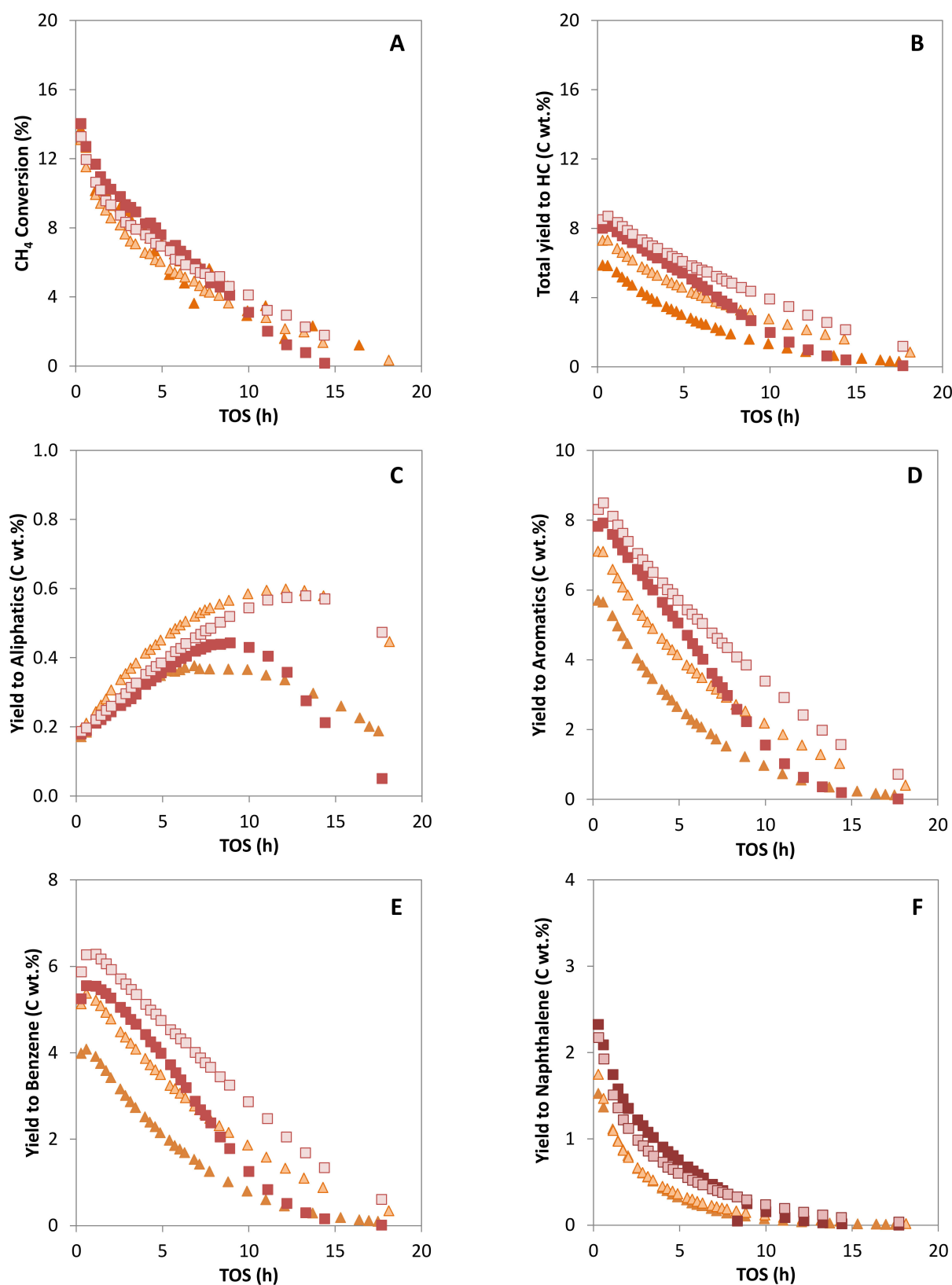


**Figure 6.** Methane conversion (A), total yield to hydrocarbons products (B), yield to aliphatics hydrocarbons (C), to aromatics hydrocarbons (D), to benzene (E) and to naphthalene (F) versus time on stream (TOS) for the catalysts: MoZ5-SSR-DC (▲), MoZ5-SSR-SC-N<sub>2</sub> (△), MoZ5-SSR-DC (■) and MoZ5-SSR-DC-N<sub>2</sub> (□), at 973 K and atmospheric pressure (w/F = 16 g·h/mol).

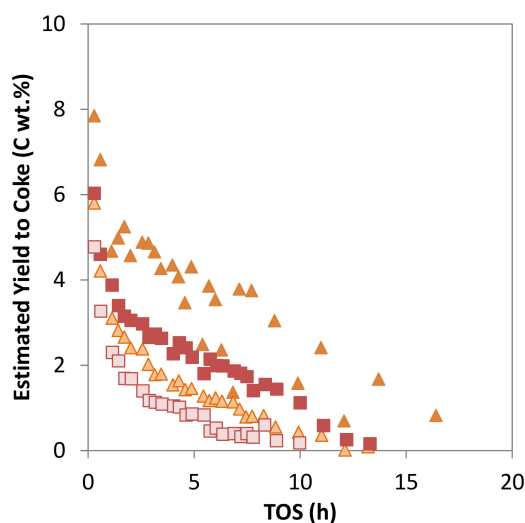


**Figure 7.** Estimated yield to coke versus time on stream (TOS) for the catalysts: MoZ5-SSR-DC ( $\blacktriangle$ ), MoZ5-SSR-SC-N<sub>2</sub> ( $\blacktriangle$ ), MoZ5-SSR-DC ( $\blacksquare$ ) and MoZ5-SSR-DC-N<sub>2</sub> ( $\square$ ), at 973 K and atmospheric pressure ( $w/F = 16 \text{ g}\cdot\text{h}/\text{mol}$ ).

#### 4. Conclusions

This work describes the influence of the different steps involved in the preparation of a Mo/ZSM-5 catalysts for dehydroaromatization of methane. Both the Mo incorporation method, e.g., by incipient wetness impregnation (IW) or by solid state ion exchange (SSR), and the calcination conditions, under static or dynamic air atmosphere, determine the size and location of the starting MoO<sub>3</sub> particles, and lead to catalysts with different micropore volume and BAS density. Thus, when the metal is added by means of IW the MoO<sub>3</sub> clusters are better dispersed on the external surface of the zeolite and a larger proportion of Mo species have migrated into the zeolite micropores, independently of the calcination procedure. However, calcination in air flow favors the formation of cationic Mo species in zeolite ion exchange positions, as suggested by the decrease of the BAS density, and in Mo species easily reducible, not only from Mo<sup>6+</sup> to Mo<sup>4+</sup>, but also from Mo<sup>4+</sup> to Mo<sup>0</sup>. On the other hand, Mo incorporation by SSR results in a poor dispersion and large MoO<sub>3</sub> clusters, especially when the samples are calcined in a muffle under static conditions. Calcination in air flow favors dispersion of the MoO<sub>3</sub> particles, but in this case the optimum Mo speciation is achieved by means of a pretreatment increasing temperature up to in a N<sub>2</sub> flow.

Regarding the performance of the different catalysts for methane dehydroaromatization, the initial conversion obtained with all samples is comparable and close to the equilibrium conversion at the reaction temperature of 973 K. However, the samples obtained by dynamic calcination in air flow, present a lower deactivation rate with TOS and higher yield to the desired aromatic hydrocarbons and, in particular, to benzene, independently of the Mo incorporation method. The catalyst performance of MoZ5-SSR-DC, prepared by solid ion exchange, can be further improved by means of the N<sub>2</sub> pretreatment, an improvement that has been directly related to the increased migration of the Mo species into the zeolite structure. Important benefits are observed, not only in catalyst life and yield to aromatics, but also in a significantly lower coke yield.

**Supplementary Materials:** The following are available online at <https://www.mdpi.com/article/10.3390/app11125465/s1>, Figure S1. FESEM images of the parent ZSM-5 zeolite, Figure S2. N<sub>2</sub> adsorption isotherms of the parent ZSM-5 zeolite and the Mo-loaded catalysts. (A) Samples prepared by incipient wetness impregnation (IW); (B) samples prepared by solid state reaction (SSR), Figure S3. SEM images using a secondary electron detector (A) and a backscattered electron detector (B) for the MoZ5-SSR-SC catalyst after being analyzed by H<sub>2</sub>-TPR, Figure S4. PXRD patterns of the Mo/ZSM-5 catalysts prepared by solid state ion exchange reaction (SSR). The most characteristic peaks related to

the presence of MoO<sub>3</sub> are marked with a dotted line, Figure S5. H<sub>2</sub>-TPR profiles for the Mo/ZSM-5 catalyst prepared by solid state ion exchange reaction calcined in static conditions (A), MoZ5-SSR-SC (black line) and MoZ5-SSR-SC-N<sub>2</sub> (grey line), and in dynamic conditions (B), MoZ5-SSR-DC (black line) and MoZ5-SSR-DC-N<sub>2</sub> (grey line).

**Author Contributions:** Conceptualization, M.T.P., C.M.; methodology, M.T.P.; investigation, M.T.P.; writing—original draft preparation, M.T.P., C.M.; writing—review and editing, F.J.L., M.M., C.M.; supervision, F.J.L., C.M.; project administration, M.M., C.M.; funding acquisition, M.M., C.M. All authors have read and agreed to the published version of the manuscript.

**Funding:** This work has been supported by the Spanish Government-MICINN through “Severo Ochoa” (SEV-2016-0683, MINECO) and RTI2018-101033-B-I00 (MCIU/AEI/FEDER, UE), and by Generalitat Valenciana (AICO/2019/060). The authors thank B. Esparcia for technical assistance and the electron Microscopy Service of the UPV for their help in sample characterization.

**Institutional Review Board Statement:** Not applicable.

**Informed Consent Statement:** Not applicable.

**Acknowledgments:** This work has been supported by the Spanish Government-MICINN through “Severo Ochoa” (SEV-2016-0683, MINECO) and RTI2018-101033-B-I00 (MCIU/AEI/FEDER, UE), and by Generalitat Valenciana (AICO/2019/060). The authors thank B. Esparcia for technical assistance and the Electron Microscopy Service of the UPV for their help in sample characterization.

**Conflicts of Interest:** The authors declare no conflict of interest.

## References

1. Gu, F.; Guo, J.; Zhang, W.; Summers, P.A.; Hall, P. From waste plastics to industrial raw materials: A life cycle assessment of mechanical plastic recycling practice based on a real-world case study. *Sci. Total Environ.* **2017**, *601–602*, 1192–1207. [[CrossRef](#)]
2. Constantinescu, M.; Bucura, F.; Ionete, E.I.; Ion-Ebrasu, D.; Sandru, C.; Zaharioiu, A.; Marin, F.; Miricioiu, M.G.; Niculescu, V.-C.; Oancea, S.; et al. From Plastic to Fuel—New Challenges. *Mater. Plast.* **2019**, *56*, 721–729. [[CrossRef](#)]
3. Constantinescu, M.; Bucura, F.; Ionete, R.-E.; Niculescu, V.-C.; Ionete, E.I.; Zaharioiu, A.; Oancea, S.; Miricioiu, M.G. Comparative Study on Plastic Materials as a New Source of Energy. *Mater. Plast.* **2019**, *56*, 41–46. [[CrossRef](#)]
4. Clauser, N.M.; González, G.; Mendieta, C.M.; Kruyeniski, J.; Area, M.C.; Vallejos, M.E. Biomass Waste as Sustainable Raw Material for Energy and Fuels. *Sustainability* **2021**, *13*. [[CrossRef](#)]
5. Varma, R.S. Biomass-Derived Renewable Carbonaceous Materials for Sustainable Chemical and Environmental Applications. *ACS Sustain. Chem. Eng.* **2019**, *7*, 6458–6470. [[CrossRef](#)]
6. Huber, G.W.; Iborra, S.; Corma, A. Synthesis of transportation fuels from biomass: Chemistry, catalysts, and engineering. *Chem. Rev.* **2006**, *106*, 4044–4098. [[CrossRef](#)] [[PubMed](#)]
7. Kondratenko, E.V.; Peppel, T.; Seeburg, D.; Kondratenko, V.A.; Kalevaru, N.; Martin, A.; Wohlrab, S. Methane conversion into different hydrocarbons or oxygenates: Current status and future perspectives in catalyst development and reactor operation. *Catal. Sci. Technol.* **2017**, *7*, 366–381. [[CrossRef](#)]
8. Schwach, P.; Pan, X.; Bao, X. Direct Conversion of Methane to Value-Added Chemicals over Heterogeneous Catalysts: Challenges and Prospects. *Chem. Rev.* **2017**, *117*, 8497–8520. [[CrossRef](#)]
9. Salvatore, A.; Gabriele, C.; Siglinda, P. Status of Research and Challenges in Converting Natural Gas. In *Small-Scale Gas to Liquid Fuel Synthesis*; CRC Press: Boca Raton, FL, USA, 2015; pp. 3–50. ISBN 978-1-4665-9938-3.
10. Perathoner, S.; Gross, S.; Hensen, E.J.M.; Wessel, H.; Chraye, H.; Centi, G. Looking at the Future of Chemical Production through the European Roadmap on Science and Technology of Catalysis the EU Effort for a Long-term Vision. *ChemCatChem* **2017**, *9*, 904–909. [[CrossRef](#)]
11. Armor, J.N. Emerging importance of shale gas to both the energy & chemicals landscape. *J. Energy Chem.* **2013**, *22*, 21–26.
12. Zhou, W.; Cheng, K.; Kang, J.; Zhou, C.; Subramanian, V.; Zhang, Q.; Wang, Y. New horizon in C<sub>1</sub> chemistry: Breaking the selectivity limitation in transformation of syngas and hydrogenation of CO<sub>2</sub> into hydrocarbon chemicals and fuels. *Chem. Soc. Rev.* **2019**, *48*, 3193–3228. [[CrossRef](#)]
13. Roberts, C.B.; Elbashir, N.O. An overview to “advances in C<sub>1</sub> chemistry in the year 2002”. *Fuel Process. Technol.* **2003**, *83*, 1–9. [[CrossRef](#)]
14. Wang, S.; Agirrezabal-Telleria, I.; Bhan, A.; Simonetti, D.; Takanebe, K.; Iglesia, E. Catalytic routes to fuels from C<sub>1</sub> and oxygenate molecules. *Faraday Discuss.* **2017**, *197*, 9–39. [[CrossRef](#)] [[PubMed](#)]
15. Lunsford, J.H. Catalytic conversion of methane to more useful chemicals and fuels: A challenge for the 21st century. *Catal. Today* **2000**, *63*, 165–174. [[CrossRef](#)]
16. Al Abdullah, M.; Rodriguez Gomez, A.; Vittenet, J.; Bendjeriou-Sedjerari, A.; Xu, W.; Abba, I.A.; Gascon, J. A Viewpoint on the Refinery of the Future: Catalyst and Process Challenges. *ACS Catal.* **2020**, *10*, 8131–8140. [[CrossRef](#)]

17. Caballero, A.; Pérez, P.J. Methane as raw material in synthetic chemistry: The final frontier. *Chem. Soc. Rev.* **2013**, *42*, 8809–8820. [[CrossRef](#)]
18. Aasberg-Petersen, K.; Dybkjær, I.; Ovesen, C.V.; Schjødt, N.C.; Sehested, J.; Thomsen, S.G. Natural gas to synthesis gas—Catalysts and catalytic processes. *J. Nat. Gas Sci. Eng.* **2011**, *3*, 423–459. [[CrossRef](#)]
19. Baliban, R.C.; Elia, J.A.; Floudas, C.A. Novel Natural Gas to Liquids Processes: Process Synthesis and Global Optimization Strategies. *AIChE J.* **2013**, *59*, 505–531. [[CrossRef](#)]
20. Sousa-Aguiar, E.F.; Appel, L.G.; Mota, C. Natural gas chemical transformations: The path to refining in the future. *Catal. Today* **2005**, *101*, 3–7. [[CrossRef](#)]
21. Gharibi, M.; Zangeneh, F.T.; Yaripour, F.; Sahebdehfar, S. Nanocatalysts for conversion of natural gas to liquid fuels and petrochemical feedstocks. *Appl. Catal. A Gen.* **2012**, *443–444*, 8–26. [[CrossRef](#)]
22. Martínez, A.; Prieto, G.; García-Trenco, A.; Peris, E. Advanced catalysts based on micro- and mesoporous molecular sieves for the conversion of natural gas to fuels and chemicals. In *Zeolites and Catalysis, Synthesis, Reactions and Applications*; Cejka, J., Corma, A., Zones, S., Eds.; WILEY-VCH: Weinheim, Germany, 2010; p. 649.
23. Portilla, M.T.; Tempelman, C.H.L.; Martínez, C.; Hensen, E.J.M. New Trends in Catalyst Design for Methane Dehydroaromatization. In *Small-Scale Gas to Liquid Fuel Synthesis*; CRC Press: Boca Raton, FL, USA, 2015; pp. 263–292. ISBN 978-1-4665-9938-3.
24. Spivey, J.J.; Hutchings, G. Catalytic aromatization of methane. *Chem. Soc. Rev.* **2014**, *43*, 792–803. [[CrossRef](#)] [[PubMed](#)]
25. Weckhuysen, B.M.; Wang, D.; Rosynek, M.P.; Lunsford, J.H. Conversion of methane to benzene over transition metal ion ZSM-5 zeolites: II. Catalyst characterization by X-ray photoelectron spectroscopy. *J. Catal.* **1998**, *175*. [[CrossRef](#)]
26. Zhang, C.L.; Li, S.; Yuan, Y.; Zhang, W.X.; Wu, T.H.; Lin, L.W. Aromatization of methane in the absence of oxygen over Mo-based catalysts supported on different types of zeolites. *Catal. Lett.* **1998**, *56*, 207–213. [[CrossRef](#)]
27. Shu, Y.; Ma, D.; Xu, L.; Bao, X.; Xu, Y. Effect of pore ring number of zeolites on catalytic performance of Mo/zeolite in methane aromatization under non-oxygen condition. *Chin. J. Catal.* **2002**, *23*, 24–28.
28. Wang, L.; Tao, L.; Xie, M.; Xu, G.; Huang, J.; Xu, Y. Dehydrogenation and aromatization of methane under non-oxidizing conditions. *Catal. Lett.* **1993**, *21*, 35–41. [[CrossRef](#)]
29. Ismagilov, Z.R.; Matus, E.V.; Kerzhentsev, M.A.; Tsikoza, L.T.; Ismagilov, I.Z.; Dosumov, K.D.; Mustafin, A.G. Methane conversion to valuable chemicals over nanostructured Mo/ZSM-5 catalysts. *Pet. Chem.* **2011**, *51*, 174–186. [[CrossRef](#)]
30. Ismagilov, Z.R.; Matus, E.V.; Tsikoza, L.T. Direct conversion of methane on Mo/ZSM-5 catalysts to produce benzene and hydrogen: Achievements and perspectives. *Energy Environ. Sci.* **2008**, *1*, 526–541. [[CrossRef](#)]
31. Wei, W. Direct dehydroaromatization of methane. *J. Nat. Gas Chem.* **2000**, *9*, 76–86.
32. Bai, J.; Liu, S.; Xie, S.; Xu, L.; Lin, L. Comparison of 6Mo/MCM-22 and 6Mo/ZSM-5 in the MDA process. *React. Kinet. Catal. Lett.* **2004**, *82*, 279–286. [[CrossRef](#)]
33. Ma, D.; Shu, Y.; Han, X.; Liu, X.; Xu, Y.; Bao, X. Mo/HMCM-22 catalysts for methane dehydroaromatization: A multinuclear MAS NMR study. *J. Phys. Chem. B* **2001**, *105*, 1786–1793. [[CrossRef](#)]
34. Majhi, S.; Mohanty, P.; Wang, H.; Pant, K.K. Direct conversion of natural gas to higher hydrocarbons: A review. *J. Energy Chem.* **2013**, *22*, 543–554. [[CrossRef](#)]
35. Shu, Y.; Ma, D.; Xu, L.; Xu, Y.; Bao, X. Methane dehydro-aromatization over Mo/MCM-22 catalysts: A highly selective catalyst for the formation of benzene. *Catal. Lett.* **2000**, *70*, 67–73. [[CrossRef](#)]
36. Sobalík, Z.; Tvarůžková, Z.; Wichterlová, B.; Fila, V.; Špatenka, Š. Acidic and catalytic properties of Mo/MCM-22 in methane aromatization: An FTIR study. *Appl. Catal. A Gen.* **2003**, *253*, 271–282. [[CrossRef](#)]
37. Shu, Y.; Ohnishi, R.; Ichikawa, M. A highly selective and coking-resistant catalyst for methane dehydrocondensation. *Chem. Lett.* **2002**, 418–419. [[CrossRef](#)]
38. Smiešková, A.; Hudec, P.; Kumar, N.; Salmi, T.; Murzin, D.Y.; Jorík, V. Aromatization of methane on Mo modified zeolites: Influence of the surface and structural properties of the carriers. *Appl. Catal. A Gen.* **2010**, *377*, 83–91. [[CrossRef](#)]
39. Liu, H.; Wu, S.; Guo, Y.; Shang, F.; Yu, X.; Ma, Y.; Xu, C.; Guan, J.; Kan, Q. Synthesis of Mo/IM-5 catalyst and its catalytic behavior in methane non-oxidative aromatization. *Fuel* **2011**, *90*, 1515–1521. [[CrossRef](#)]
40. Liu, H.; Hu, J.; Li, Z.; Wu, S.; Liu, L.; Guan, J.; Kan, Q. Synthesis of zeolite IM-5 under rotating and static conditions and the catalytic performance of Mo/H-IM-5 catalyst in methane non-oxidative aromatization. *Kinet. Catal.* **2013**, *54*, 443–450. [[CrossRef](#)]
41. Portilla, M.T.; Llopis, F.J.; Martinez, C. Non-oxidative dehydroaromatization of methane: An effective reaction-regeneration cyclic operation for catalyst life extension. *Catal. Sci. Technol.* **2015**, *5*, 3806–3821. [[CrossRef](#)]
42. Liu, H.; Yang, S.; Wu, S.; Shang, F.; Yu, X.; Xu, C.; Guan, J.; Kan, Q. Synthesis of Mo/TNU-9 (TNU-9 Taejon National University No. 9) catalyst and its catalytic performance in methane non-oxidative aromatization. *Energy* **2011**, *36*, 1582–1589. [[CrossRef](#)]
43. Ma, S.; Guo, X.; Zhao, L.; Scott, S.; Bao, X. Recent progress in methane dehydroaromatization: From laboratory curiosities to promising technology. *J. Energy Chem.* **2013**, *22*, 1–20. [[CrossRef](#)]
44. Kosinov, N.; Hensen, E.J.M. Reactivity, Selectivity, and Stability of Zeolite-Based Catalysts for Methane Dehydroaromatization. *Adv. Mater.* **2020**, *32*, 2002565. [[CrossRef](#)] [[PubMed](#)]
45. Vollmer, I.; Ould-Chikh, S.; Aguilar-Tapia, A.; Li, G.; Pidko, E.; Hazemann, J.-L.; Kapteijn, F.; Gascon, J. Activity Descriptors Derived from Comparison of Mo and Fe as Active Metal for Methane Conversion to Aromatics. *J. Am. Chem. Soc.* **2019**, *141*, 18814–18824. [[CrossRef](#)]

46. Çağlayan, M.; Lucini Paioni, A.; Abou-Hamad, E.; Shterk, G.; Pustovarenko, A.; Baldus, M.; Chowdhury, A.D.; Gascon, J. Initial Carbon–Carbon Bond Formation during the Early Stages of Methane Dehydroaromatization. *Angew. Chem. Int. Ed.* **2020**, *59*, 16741–16746. [[CrossRef](#)] [[PubMed](#)]
47. Vollmer, I.; Gascon, J.; Kapteijn, F.; Yarulina, I.; Olivos Suarez, A.I.; van der Linden, B.; Sneider, Y.G. On the dynamic nature of Mo sites for methane dehydroaromatization. In Proceedings of the Abstracts of Papers, 255th ACS National Meeting & Exposition, New Orleans, LA, USA, 18–22 March 2018; American Chemical Society: Washington, DC, USA, 2018; p. CATL-135.
48. Li, G.; Vollmer, I.; Liu, C.; Gascon, J.; Pidko, E.A. Structure and Reactivity of the Mo/ZSM-5 Dehydroaromatization Catalyst: An Operando Computational Study. *ACS Catal.* **2019**, *9*, 8731–8737. [[CrossRef](#)]
49. Vollmer, I.; Mondal, A.; Yarulina, I.; Abou-hamad, E.; Kapteijn, F.; Gascon, J. Quantifying the impact of dispersion, acidity and porosity of Mo/HZSM-5 on the performance in methane dehydroaromatization. *Appl. Catal. A Gen.* **2019**, *574*, 144–150. [[CrossRef](#)]
50. Borry, R.W.; Kim, Y.H.; Huffsmith, A.; Reimer, J.A.; Iglesia, E. Structure and density of Mo and acid sites in Mo-exchanged H-ZSM5 catalysts for nonoxidative methane conversion. *J. Phys. Chem. B* **1999**, *103*, 5787–5796. [[CrossRef](#)]
51. Liu, H.; Shen, W.; Bao, X.; Xu, Y. Identification of Mo active species for methane dehydro-aromatization over Mo/HZSM-5 catalysts in the absence of oxygen: 1H MAS NMR and EPR investigations. *J. Mol. Catal. A Chem.* **2006**, *244*, 229–236. [[CrossRef](#)]
52. Liu, H.; Bao, X.; Xu, Y. Methane dehydroaromatization under nonoxidative conditions over Mo/HZSM-5 catalysts: Identification and preparation of the Mo active species. *J. Catal.* **2006**, *239*, 441–450. [[CrossRef](#)]
53. Lacheen, H.S.; Iglesia, E. Isothermal activation of Mo2O5 2+-ZSM-5 precursors during methane reactions: Effects of reaction products on structural evolution and catalytic properties. *Phys. Chem. Chem. Phys.* **2005**, *7*, 538–547. [[CrossRef](#)]
54. Ding, W.; Li, S.; Meitzner, G.D.; Iglesia, E. Methane conversion to aromatics on Mo/H-ZSM5: Structure of molybdenum species in working catalysts. *J. Phys. Chem. B* **2001**, *105*, 506–513. [[CrossRef](#)]
55. Li, W.; Meitzner, G.D.; Borry, R.W.; Iglesia, E. Raman and X-ray absorption studies of Mo species in Mo/H-ZSM5 catalysts for non-oxidative CH4 reactions. *J. Catal.* **2000**, *191*, 373. [[CrossRef](#)]
56. Ding, W.; Meitzner, G.D.; Iglesia, E. The effects of silanation of external acid sites on the structure and catalytic behavior of Mo/H-ZSM5. *J. Catal.* **2002**, *206*, 14–22. [[CrossRef](#)]
57. Martínez, C.; Corma, A. Inorganic molecular sieves: Preparation, modification and industrial application in catalytic processes. *Coord. Chem. Rev.* **2011**, *255*, 1558–1580. [[CrossRef](#)]
58. Xu, Y.; Shu, Y.; Liu, S.; Huang, J.; Guo, X. Interaction between ammonium heptamolybdate and NH4ZSM-5 zeolite: The location of Mo species and the acidity of Mo/HZSM-5. *Catal. Lett.* **1995**, *35*, 233–243. [[CrossRef](#)]
59. Kim, Y.; Borry, R.W.; Iglesia, E. Genesis of methane activation sites in Mo-exchanged H—ZSM-5 catalysts. *Microporous Mesoporous Mater.* **2000**, *36*, 495–509. [[CrossRef](#)]
60. Zheng, H.; Ma, D.; Bao, X.; Jian, Z.H.; Ja, H.K.; Wang, Y.; Peden, C.H.F. Direct observation of the active center for methane dehydroaromatization using an ultrahigh field 95Mo NMR spectroscopy. *J. Am. Chem. Soc.* **2008**, *130*, 3722–3723. [[CrossRef](#)] [[PubMed](#)]
61. Vollmer, I.; Yarulina, I.; Kapteijn, F.; Gascon, J. Progress in Developing a Structure–Activity Relationship for the Direct Aromatization of Methane. *ChemCatChem* **2019**, *11*, 39–52. [[CrossRef](#)]
62. Gao, J.; Zheng, Y.; Jehng, J.-M.; Tang, Y.; Wachs, I.E.; Podkolzin, S.G. Identification of molybdenum oxide nanostructures on zeolites for natural gas conversion. *Science* **2015**, *348*, 686–690. [[CrossRef](#)]
63. Kosinov, N.; Coumans, F.J.A.G.; Uslamin, E.A.; Wijpkema, A.S.G.; Mezari, B.; Hensen, E.J.M. Methane Dehydroaromatization by Mo/HZSM-5: Mono- or Bifunctional Catalysis? *ACS Catal.* **2017**, *7*, 520–529. [[CrossRef](#)]
64. Liu, S.; Wang, L.; Ohnishi, R.; Ichikawa, M. Bifunctional catalysis of Mo/HZSM-5 in the dehydroaromatization of methane to benzene and naphthalene XAFS/TG/DTA/ MASS/FTIR characterization and supporting effects. *J. Catal.* **1999**, *181*, 175–188. [[CrossRef](#)]
65. Su, L.; Xu, Y.; Bao, X. Study on Bifunctionality of Mo/HZSM-5 Catalysts for Methane Dehydro-Aromatization under Non-oxidative Condition. *J. Nat. Gas Chem.* **2002**, *11*, 18–27.
66. Kosinov, N.; Wijpkema, A.S.G.; Uslamin, E.; Rohling, R.; Coumans, F.J.A.G.; Mezari, B.; Parastaev, A.; Poryvaev, A.S.; Fedin, M.V.; Pidko, E.A.; et al. Confined Carbon Mediating Dehydroaromatization of Methane over Mo/ZSM-5. *Angew. Chem. Int. Ed.* **2018**, *57*, 1016–1020. [[CrossRef](#)]
67. Kosinov, N.; Uslamin, E.A.; Coumans, F.J.A.G.; Wijpkema, A.S.G.; Rohling, R.Y.; Hensen, E.J.M. Structure and Evolution of Confined Carbon Species during Methane Dehydroaromatization over Mo/ZSM-5. *ACS Catal.* **2018**, *8*, 8459–8467. [[CrossRef](#)] [[PubMed](#)]
68. Li, B.; Li, S.; Li, N.; Chen, H.; Zhang, W.; Bao, X.; Lin, B. Structure and acidity of Mo/ZSM-5 synthesized by solid state reaction for methane dehydrogenation and aromatization. *Microporous Mesoporous Mater.* **2006**, *88*, 244–253. [[CrossRef](#)]
69. Sedel’nikova, O.V.; Stepanov, A.A.; Zaikovskii, V.I.; Korobitsyna, L.L.; Vosmerikov, A.V. Preparation method effect on the physicochemical and catalytic properties of a methane dehydroaromatization catalyst. *Kinet. Catal.* **2017**, *58*, 51–57. [[CrossRef](#)]
70. Brunauer, S.; Emmett, P.H.; Teller, E. Adsorption of Gases in Multimolecular Layers. *J. Am. Chem. Soc.* **1938**, *60*, 309–319. [[CrossRef](#)]



71. Harkins, W.D.; Jura, G. Surfaces of Solids. XIII. A Vapor Adsorption Method for the Determination of the Area of a Solid without the Assumption of a Molecular Area, and the Areas Occupied by Nitrogen and Other Molecules on the Surface of a Solid. *J. Am. Chem. Soc.* **1944**, *66*, 1366–1373. [[CrossRef](#)]
72. Emeis, C.A. Determination of Integrated Molar Extinction Coefficients for Infrared Absorption Bands of Pyridine Adsorbed on Solid Acid Catalysts. *J. Catal.* **1993**, *141*, 347–354. [[CrossRef](#)]
73. Martínez, A.; Peris, E.; Derewinski, M.; Burkat-Dulak, A. Improvement of catalyst stability during methane dehydroaromatization (MDA) on Mo/HZSM-5 comprising intracrystalline mesopores. *Catal. Today* **2011**, *169*, 75–84. [[CrossRef](#)]
74. Li, W.; Meitzner, G.D.; Kim, Y.H.; Borry, R.W.; Iglesia, E. The location, structure, and role of MoO and MoC species in Mo/H-ZSM5 catalysts for methane aromatization. *Stud. Surf. Sci. Catal.* **2000**, *130 D*, 3621–3626.
75. Song, Y.; Sun, C.; Shen, W.; Lin, L. Hydrothermal post-synthesis of HZSM-5 zeolite to enhance the coke-resistance of Mo/HZSM-5 catalyst for methane dehydroaromatization. *Catal. Lett.* **2006**, *109*, 21–24. [[CrossRef](#)]
76. Jin, Z.; Liu, S.; Qin, L.; Liu, Z.; Wang, Y.; Xie, Z.; Wang, X. Methane dehydroaromatization by Mo-supported MFI-type zeolite with core-shell structure. *Appl. Catal. A Gen.* **2013**, *453*, 295–301. [[CrossRef](#)]
77. Ding, W.; Meitzner, G.D.; Marler, D.O.; Iglesia, E. Synthesis, structural characterization, and catalytic properties of tungsten-exchanged H-ZSM5. *J. Phys. Chem. B* **2001**, *105*, 3928–3936. [[CrossRef](#)]
78. Bijani, P.M.; Sohrabi, M.; Sahebdehfar, S. Thermodynamic Analysis of Nonoxidative Dehydroaromatization of Methane. *Chem. Eng. Technol.* **2012**, *35*, 1825–1832. [[CrossRef](#)]